Disease Models & Mechanisms 6, 608-621 (2013) doi:10.1242/dmm.010900

Neurons and cardiomyocytes derived from induced pluripotent stem cells as a model for mitochondrial defects in Friedreich's ataxia

Aurore Hick[1,2,3,4,5,*], Marie Wattenhofer-Donzé[1,2,3,4,5,*], Satyan Chintawar[6,*], Philippe Tropel[2,3,4,7,‡], Jodie P. Simard[8], Nadège Vaucamps[1,2,3,4,5], David Gall[9], Laurie Lambot[9], Cécile André[2,3,4,7], Laurence Reutenauer[1,2,3,4,5], Myriam Rai[6], Marius Teletin[2,3,4,7], Nadia Messaddeq[1,2,3,4,5], Serge N. Schiffmann[9], Stéphane Viville[2,3,4,7], Christopher E. Pearson[8,10], Massimo Pandolfo[6,11,§] and Hélène Puccio[1,2,3,4,5,§]

SUMMARY

Friedreich's ataxia (FRDA) is a recessive neurodegenerative disorder commonly associated with hypertrophic cardiomyopathy. FRDA is due to expanded GAA repeats within the first intron of the gene encoding frataxin, a conserved mitochondrial protein involved in iron-sulphur cluster biosynthesis. This mutation leads to partial gene silencing and substantial reduction of the frataxin level. To overcome limitations of current cellular models of FRDA, we derived induced pluripotent stem cells (iPSCs) from two FRDA patients and successfully differentiated them into neurons and cardiomyocytes, two affected cell types in FRDA. All FRDA iPSC lines displayed expanded GAA alleles prone to high instability and decreased levels of frataxin, but no biochemical phenotype was observed. Interestingly, both FRDA iPSC-derived neurons and cardiomyocytes exhibited signs of impaired mitochondrial function, with decreased mitochondrial membrane potential and progressive mitochondrial degeneration, respectively. Our data show for the first time that FRDA iPSCs and their neuronal and cardiac derivatives represent promising models for the study of mitochondrial damage and GAA expansion instability in FRDA.

INTRODUCTION

Friedreich's ataxia (FRDA), the most prevalent hereditary ataxia in Caucasians, is a multisystem autosomal recessive disorder with neurological and cardiac involvement dominating the clinical picture (Pandolfo, 2009). Atrophy of sensory and cerebellar pathways causes ataxia, dysarthria, fixation instability, deep sensory loss and loss of tendon reflexes (Pandolfo, 2009). Cardiac dysfunction leading to congestive heart failure and arrhythmias is the cause of death in 59% of FRDA patients (Tsou et al., 2011). About 10% of FRDA patients develop diabetes, but insulin resistance and β-cell dysfunction are very common (Cnop et al., 2012).

FRDA is caused by reduced expression of the mitochondrial protein, frataxin (Campuzano et al., 1997). Most individuals with FRDA are homozygous for a GAA triplet repeat expansion within the first intron of the frataxin (*FXN*) gene (Campuzano et al., 1996), which leads to partial silencing of *FXN* transcription through epigenetic mechanisms (Saveliev et al., 2003). Normal chromosomes contain up to 40 GAA repeats, whereas disease-associated alleles contain 100-1000 GAA repeats (Campuzano et al., 1996). Patients have between 5 and 35% of the frataxin levels in healthy individuals, whereas asymptomatic heterozygous subjects have >50% (Campuzano et al., 1997; Deutsch et al., 2010). The GAA repeat expansions are dynamic and exhibit both intergenerational and somatic instability (De Biase et al., 2007; Monrós et al., 1997). Progressive somatic expansion in a subset of tissues could play an important role in disease progression (Clark et al., 2007). However, the molecular mechanisms underlying GAA repeat instability are currently unknown.

Although the function of frataxin is still under investigation, available evidence supports a role as an activator of iron-sulphur (Fe-S) cluster biogenesis in mitochondria (Schmucker et al., 2011; Tsai and Barondeau, 2010). Fe-S clusters are essential prosthetic groups for many proteins with a variety of functions and subcellular localisations (Lill, 2009 ; Ye and Rouault, 2010). Frataxin deficiency leads to impairment of Fe-S cluster-containing proteins, altered cellular iron metabolism, mitochondrial dysfunction and increased sensitivity to oxidative stress (Schmucker and Puccio, 2010), but

[1]Translational Medicine and Neurogenetics, Institut de Génétique et de Biologie Moléculaire et Cellulaire (IGBMC), 67404 Illkirch, France
[2]INSERM, U596, 67404 Illkirch, France
[3]CNRS, UMR7104, 67404 Illkirch, France
[4]Université de Strasbourg, 67000 Strasbourg, France
[5]Collège de France, Chaire de génétique humaine, 67404 Illkirch, France
[6]Laboratoire de Neurologie Expérimentale, Université Libre de Bruxelles (ULB), Brussels, Belgium
[7]Development and Stem Cells, Institut de Génétique et de Biologie Moléculaire et Cellulaire (IGBMC), 67404 Illkirch, France
[8]Program of Genetics and Genome Biology, The Hospital for Sick Children, Toronto, ON, M5G 1L7, Canada
[9]Laboratoire de Neurophysiologie, Université Libre de Bruxelles (ULB), 1050 Brussels, Belgium
[10]Department of Molecular Genetics, University of Toronto, Toronto, ON, M5G 1L7, Canada
[11]Service de Neurologie, Hôpital Erasme, 1070 Brussels, Belgium
*These authors should be regarded as joint first authors
‡Present address: Aix-Marseille Université, INSERM UMR 910, Faculté de Médecine Timone, 13385, Marseille, France
§Authors for correspondence (massimo.pandolfo@ulb.ac.be; hpuccio@igbmc.fr)

Received 19 September 2012; Accepted 6 November 2012

TRANSLATIONAL IMPACT

Clinical issue

Friedreich's ataxia (FRDA), an autosomal recessive multisystem disorder characterised by neurodegeneration and cardiomyopathy, is caused by reduced levels of frataxin, an essential mitochondrial protein. Most individuals with FRDA are homozygous for an expanded GAA repeat in the first intron of the frataxin gene (*FXN*); this leads to repressed *FXN* expression through epigenetic mechanisms. Animal models of FRDA have enabled substantial progress in understanding pathogenesis, but none fully recapitulates the genetic and epigenetic characteristics of the human disease. Moreover, easily accessible cells from patients do not show any phenotype.

Results

The aim of this study was to generate induced pluripotent stem cells (iPSCs) from individuals with FRDA and differentiate them into neuronal and cardiac lineages. The authors successfully derived iPSCs from two FRDA patients. Both sets of IPSCs displayed expanded GAA repeats that were prone to high instability and decreased levels of frataxin, but no biochemical phenotype. In addition, FRDA iPSCs did not differ from control iPSCs with respect to morphology and differentiation potential. The authors then differentiated these iPSCs into neurons and cardiomyocytes. FRDA iPSC-derived committed neural precursor cells and differentiated neurons did not differ morphologically from controls, even at the ultrastructural level. However, FRDA iPSC-derived neurons showed signs of mitochondrial defects and delayed electrophysiological maturation compared with control iPSC-derived neurons. FRDA iPSC-derived cardiomyocytes also exhibited signs of impaired mitochondrial homeostasis. Expanded GAA repeats, which were very unstable in iPSCs, became much more stable upon differentiation. Levels of mismatch repair factors MSH2 and MSH6, considered to be involved in repeat instability, were much higher in iPSCs than in fibroblasts used for reprogramming, both in FRDA and control subjects. However, expression of these factors also remained high during differentiation, suggesting that other factors also play a role in repeat instability.

Implications and future directions

Patient-derived iPSCs and their derived differentiated cells can be maintained in long-term culture and constitute a permanent source of differentiated cells. These cells are an important resource for research into FRDA pathogenesis and provide an excellent system for testing potential therapeutics, as they fully recapitulate the genetic aspects of the disease and express detectable, measurable phenotypes. The phenotypes characterised in this study for differentiated neurons and cardiomyocytes can be further dissected to identify underlying molecular mechanisms, which appear to involve altered mitochondrial homeostasis. Guiding differentiation toward specific neuronal types that are particularly vulnerable in FRDA (cerebellar deep nuclei and primary sensory neurons) will soon be possible as specific protocols are developed.

the relative contribution of these mechanisms to pathogenesis is not yet defined.

The genetic basis of FRDA challenges the development of models, yet required to understand the disease mechanisms and design drug screening assays. The currently available mouse models are either mildly symptomatic (Al-Mahdawi et al., 2006; Miranda et al., 2002) or tissue-specific knockouts (Puccio et al., 2001; Simon et al., 2004). Cellular models include easily obtained, but unaffected cells from FRDA patients, engineered cell lines with frataxin knockdown and cells derived from animal models (Martelli et al., 2012). These models have allowed important advances in understanding frataxin function and pathogenesis, and have been used to test drug effects (Martelli et al., 2012). However, none of them faithfully recapitulates the human disease, and no long-term cultures of mutated vulnerable human cells, such as neurons and cardiomyocytes, are available. Reprogramming of somatic cells to generate pluripotent stem cells (induced pluripotent stem cells, iPSCs) provides a long-term source for deriving any cell type genetically identical to the original somatic cell. Accordingly, iPSCs have been used to obtain cultures of vulnerable cells in genetic diseases (Onder and Daley, 2012). Recently, two groups reported the successful generation of FRDA iPSCs (Ku et al., 2010; Liu et al., 2011). These iPSCs show epigenetic silencing of the *FXN* locus (Ku et al., 2010), low levels of frataxin expression (Ku et al., 2010; Liu et al., 2011) and GAA repeat instability, with only expansions (Ku et al., 2010) or both expansions and contractions (Liu et al., 2011). Furthermore, one group reports the involvement of mismatch repair (MMR) enzymes in the GAA repeat expansions (Du et al., 2012; Ku et al., 2010). However, none of these studies reported a phenotype resulting from frataxin deficiency in cells obtained from FRDA iPSCs. Here, we describe the generation and characterisation of FRDA iPSCs as well as neurons and cardiomyocytes derived from the FRDA iPSCs. We show that iPSC-derived neurons and cardiomyocytes from FRDA patients maintain GAA repeat expansions of pathological size and express low levels of frataxin compared with control cells, resulting in neuronal and cardiac mitochondrial abnormalities and delayed functional maturation of neurons. Furthermore, we found high levels of GAA instability, both expansions and contractions, in the FRDA iPSCs, which correlates with an upregulation of the MMR enzymes MSH2, MSH3 and MSH6 upon reprogramming. Our findings confirm the mitochondrial pathogenesis of FRDA and provide cellular phenotypes to test potential therapeutics.

RESULTS

Generation and characterisation of iPSC lines from FRDA patient fibroblasts

Dermal fibroblasts were obtained from two patients with FRDA and two age-matched unrelated healthy individuals after informed consent (see Materials and Methods). Fibroblasts from FRDA patients (FD135 and FD141) had expanded GAA repeats (800/600 and 900/400, respectively) whereas the control fibroblasts (CT136 and CT145) had normal GAA repeats (<20) (Fig. 1A). To obtain iPSCs, the fibroblasts were transduced with lentivirus expressing the reprogramming factors OCT4, SOX2, LIN28 and NANOG as described previously (Lapillonne et al., 2010). At 4-6 weeks after transduction, 5-15 independent iPSC colonies per cell line were manually picked on the basis of their human embryonic stem cell (hESC)-like morphology. The expanded GAA repeats length was determined on each clone prior to full characterisation. All iPSC clones derived from FRDA patients retained pathological GAA repeat expansions, ranging between 400 and 1000 triplets (Fig. 1A), with the exception of one clone, in which one allele contracted to 200 GAA triplets, a size still within the pathological range (FD135-4L clone 28; Fig. 1A).

All iPSC clones stained for the pluripotency markers TRA1-60, TRA1-81 and NANOG (Fig. 1B), most silenced the transduced *OCT4*, *SOX2*, *NANOG* and *LIN28* genes and expressed the corresponding endogenous genes (supplementary material Fig. S1A,B). They also showed extensive DNA demethylation at the proximal promoter and the distal enhancer of the endogenous *OCT4* locus (supplementary material Fig. S1C), demonstrating

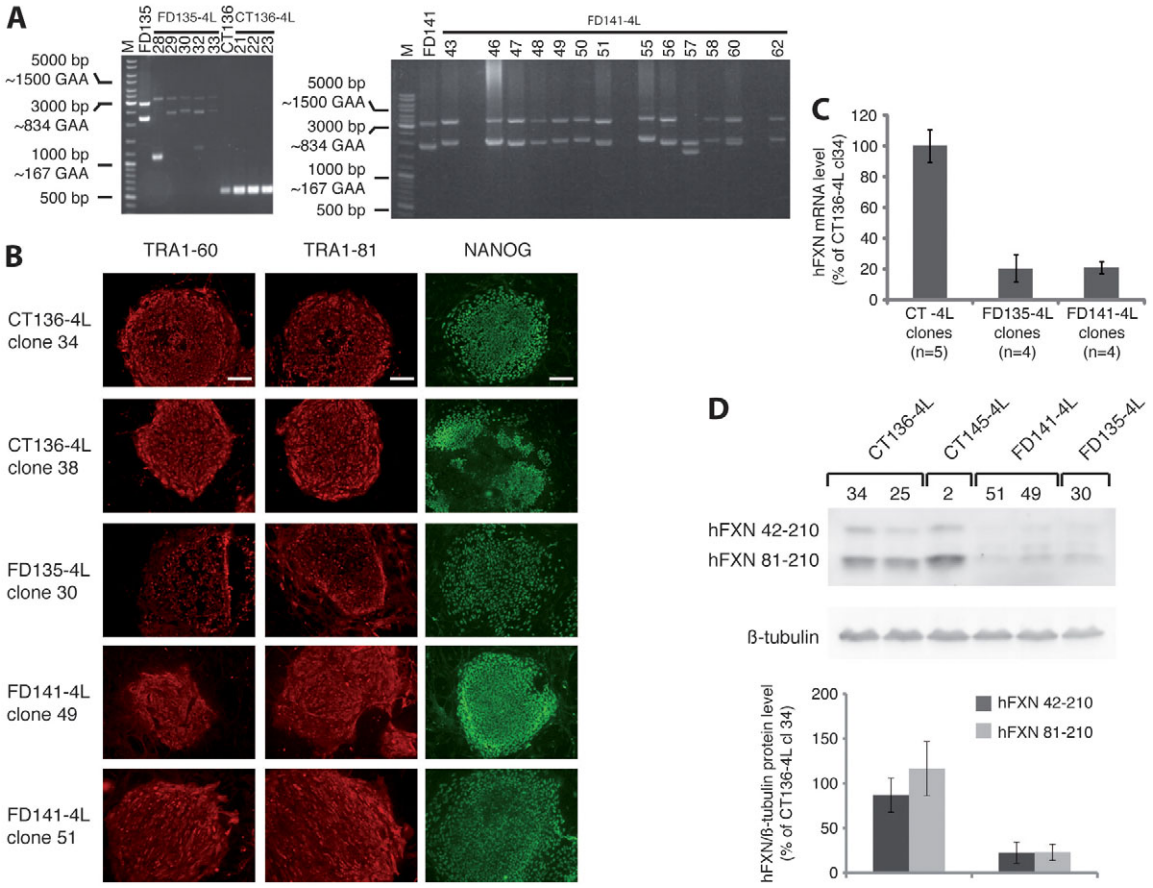

Fig. 1. Generation and characterisation of iPSC cell lines from control and FRDA fibroblasts. (A) PCR analysis of *FXN* GAA repeat length in fibroblast cell lines (FD135, CT136 and FD141) and iPSCs (FD135-4L, CT136-4L and FD141-4L clones). CT136 corresponds to an unaffected control; FD135 and FD141 correspond to two unrelated FRDA patients. Numbers represent different iPSC clones isolated for each cell lines. M, molecular weight marker. (B) Representative colonies of control and FRDA iPSCs stained positive for the pluripotency markers TRA1-60 (red), TRA1-81 (red) and NANOG (green). Scale bars: 200 µm. (C) qRT-PCR analysis of frataxin expression relative to *GADPH* in control and FRDA iPSCs. The value of CT136-4L clone 34 was arbitrarily set to 100. (D) Western blot of whole cell extracts from control or FRDA iPSCs. The intermediate (hFXN 42-210) and mature (hFXN 81-210) forms of frataxin are detected. β-tubulin is used as a loading control. Protein levels were quantified after normalisation with β-tubulin and expressed as a percentage of control level (CT136-4L clone 34 was arbitrarily set at 100); *n*=3 in each group. Data are presented as mean ± s.d.

faithful reprogramming. In addition, all iPSC clones maintained a normal karyotype. Two or three clones per line were selected for further characterisation (see supplementary material Table S1). Their pluripotency was confirmed *in vitro* by the formation of embryoid bodies (EBs) that expressed genes from all three embryonic layers (supplementary material Fig. S2). Furthermore, iPSCs were able to form teratomas in SCID mice that contained tissues derived from all three germ layers, including gut-like epithelium (endoderm), cartilage (mesoderm) and neural tissues (ectoderm) (supplementary material Fig. S3). Collectively, these results demonstrate that we successfully generated iPSCs from FRDA fibroblasts with pluripotent propensity.

We next determined whether the expanded GAA repeats in FRDA iPSCs still caused *FXN* gene silencing present in patient somatic cells (including the fibroblasts used for reprogramming). qRT-PCR analysis confirmed an ~80% decrease in *FXN* mRNA in all FRDA iPSC clones, as compared with control iPSCs (Fig. 1C). By western blot analysis, FRDA iPSCs had 23% residual frataxin compared with control iPSCs (Fig. 1D), as previously observed in various patient-derived cell lines (Deutsch et al., 2010; Selak et al., 2011). Frataxin deficiency leads to impaired Fe-S cluster biosynthesis and reduced Fe-S cluster enzyme activity in affected tissues (Martelli et al., 2007; Puccio et al., 2001; Rötig et al., 1997). The activity of the Fe-S cluster containing succinate dehydrogenase (SDH) enzyme, the levels of Fe-S dependent proteins, which normally show diminished levels of apoprotein when cells are unable to generate Fe-S clusters (Guillon et al., 2009; Martelli et al., 2007; Navarro-Sastre et al., 2011), and the levels of protein-bound lipoic acid, a cofactor that is synthesised by the Fe-S-containing enzyme lipoic acid synthase (Navarro-Sastre et al., 2011), are not affected in FRDA-derived iPSCs (supplementary material Fig. S4). Together, these results demonstrate that, as for FRDA-derived fibroblasts, despite low levels of frataxin protein in FRDA-derived iPSCs, there is no evidence of Fe-S cluster biogenesis defects.

iPSC neural differentiation

In an attempt to generate faithful cell models that recapitulate the pathophysiological features of the disease, we derived human

neurons from normal and FRDA iPSCs following an established protocol (Dottori and Pera, 2008) with slight modifications (see Materials and Methods; Fig. 2A). Treatment of iPSCs for 14 days with the bone morphogenetic protein (BMP) antagonist Noggin led to the induction of neural precursors, which were immunopositive for the neuroectodermal markers Nestin and PAX6 (Fig. 2C). Neural precursors were mechanically isolated and cultured in suspension as neurospheres, which extinguished the expression of pluripotent factors *NANOG*, *LIN28* and *OCT4* while retaining the expression of *SOX2*, a transcription factor expressed in neuronal precursors (Fig. 2B). Within 3 days of culture in differentiation conditions, neurospheres started extending processes in all directions. Over 30 days, dense networks of neurons with extended radially projecting neurites positive for the early phase neural marker β-III-tubulin were formed (Fig. 2A). These cells commonly expressed MAP2 (microtubule-associated protein 2), a dendrite specific marker in mature neurons (Fig. 2D,E). Furthermore, synapsin puncta outlining the MAP2-positive neurites became visible by immunostaining (Fig. 2D), evidence of synaptic connections. A subpopulation of neurons expressed the vesicular glutamate transporter 1/2 (VGlut1/2) (Fig. 2E), in accordance with the notion that human neural precursors in the absence of any specific cues mostly generate glutamatergic neurons (Mariani et al., 2012).

FRDA neurons demonstrate physiological and mitochondrial abnormalities

To address whether the FRDA iPSC-derived neurospheres and differentiated neurons exhibited any pathological features, we first assessed the GAA expansion and the levels of frataxin expression. Neurospheres and neurons obtained from FRDA iPSCs retained pathological GAA repeat expansions (Fig. 3B) and maintained low *FXN* mRNA expression levels, at 30-35% of controls (Fig. 3C), but showed no obvious difference in morphology, viability or differentiation potential compared with those derived from control iPSCs (Fig. 3A). However, at 34-39 days of differentiation, 30% less FRDA than control neurons exhibited spontaneous calcium transients (Fig. 2F; supplementary material Movie 1) (Fig. 3D). Patch clamp recordings from neurons participating in spontaneous calcium oscillations showed that 16/28 control cells from two clones displayed voltage-dependent sodium currents, 11 showed repetitive firing during step current injection with little or no accommodation, and five were spontaneously active (Fig. 3D). By contrast, only 6/30 recorded neurons from two FRDA clones displayed voltage-

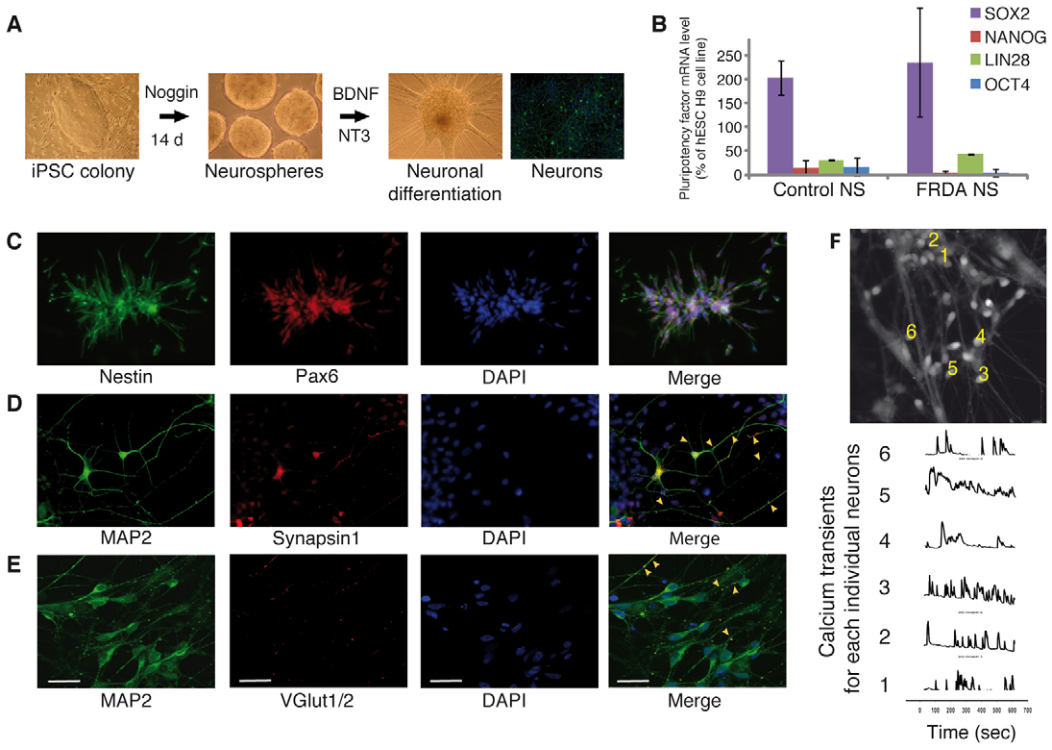

Fig. 2. Differentiation of FRDA iPSCs into neurons and their characterisation. (A) Schematic view of the neural differentiation protocol. Representative images show an iPSC colony treated with noggin for 14 days, cultured as neuropheres, and neuropheres undergoing neural differentiation in the presence of neurotrophic factors, BDNF and NT3 (bright fields) and neurons (immunostained for β-tubulin III; green). (B) qRT-PCR analysis of the expression levels of endogenous *SOX2*, *NANOG*, *LIN28* and *OCT4* relative to *GADPH* in control and FRDA neurospheres (NS) normalised to hESC H9. The data are presented as mean ± s.d. (C) Representative iPSC-derived neurospheres (FD135-4L clone 30) stained positive for the neural stem cell markers Nestin (green) and Pax6 (red). Nuclei are counterstained with DAPI (blue). The majority of cells coexpress both markers. (D,E) Representative iPSC-derived neurons at 45 days (FD135-4L clone 30) stained positive for MAP2 (green). (D) Positive labeling for synapsin1 (red) demonstrates synapse formation (see arrowheads in merge). (E) A subset of cells stain positive for the glutamate vesicular transporter VGlut1/2 (red, see arrowheads in merge). (F) Top: unprocessed fluorescence image of iPSC-derived neurons at 35 days (FD135-4L clone 30) loaded with the calcium indicator Oregon Green 488 BAPTA 1. Bottom: representative traces from numbered neurons (1-6) showing spontaneous calcium spikes. Scale bars: 20 μm.

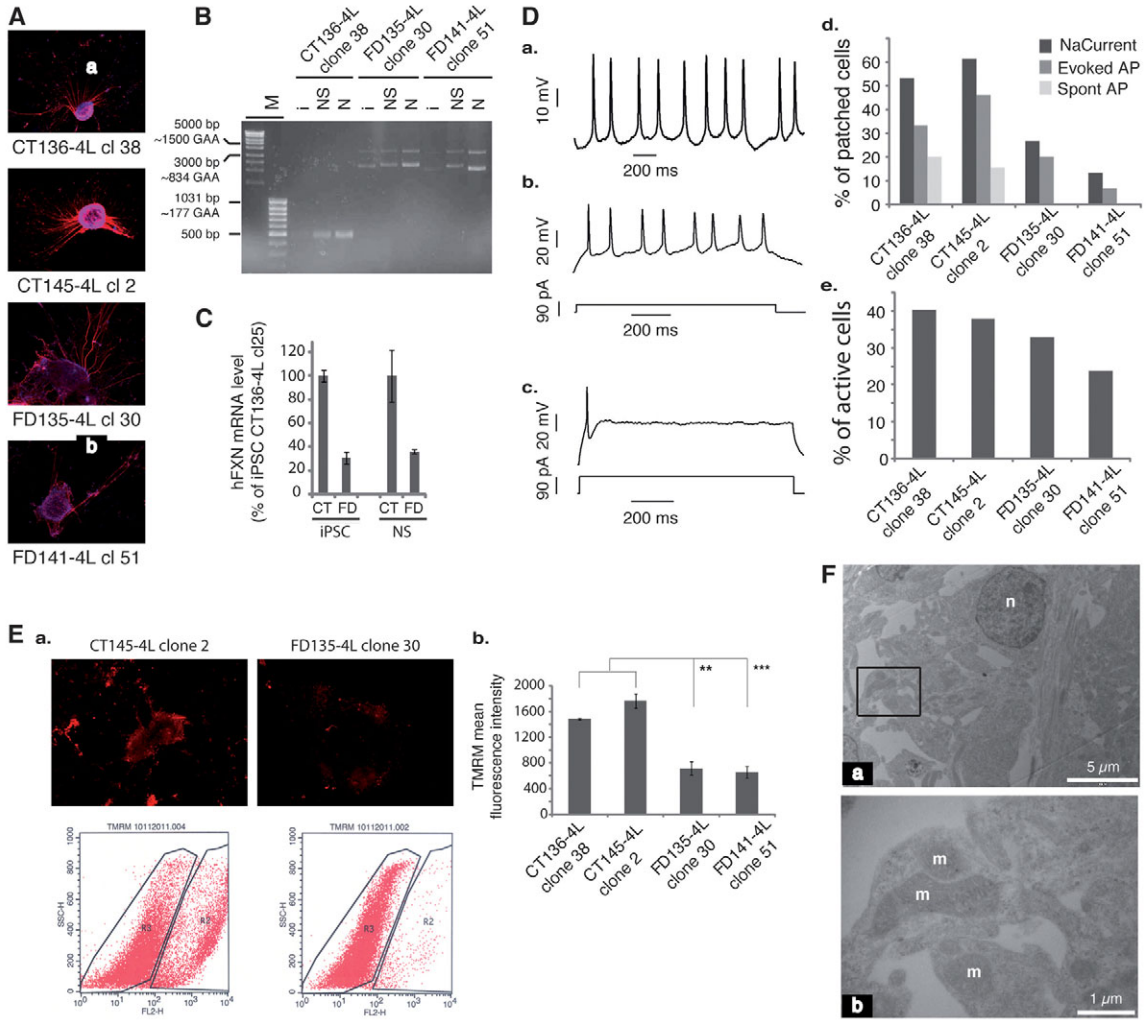

Fig. 3. FRDA neurons are functionally impaired and have reduced mitochondrial membrane potential. (A) Representative images of iPSC-derived 8-day-old differentiating neurospheres for both control and FRDA clones stained positive for β-tubulin III. (B) PCR analysis of *FXN* GAA repeat length in iPSCs, neurospheres (NS) and neurons (N) from representative control (CT136-4L clone 38) and FRDA (FD135-4L clone 30 and FD141-4L clone 51) lines. M, molecular weight marker. (C) qRT-PCR analysis of frataxin expression relative to *GADPH* in control (CT) and FRDA (FD) iPSCs and neurospheres (NS). The value of iPSC CT136-4L clone 25 was arbitrarily set to 100. The data are presented as mean ± s.d. (D) Electrophysiological characteristics of iPSC-derived neurons. Representative traces obtained from current-clamp recordings in maturating iPSC-derived neurons at days 34-39 are shown: (Da) Control neuron (CT 136-4L clone 38) showing spontaneous repetitive action potentials, a recording never detected in any FRDA neurons. (Db) Control neuron (CT 136-4L clone 38) showing repetitive depolarisation-evoked action potentials. (Dc) FRDA neuron (FD141-4L clone 51) showing a single depolarisation-evoked action potential. (Dd) Quantification of iPSC-derived control and FRDA neurons expressing voltage-dependent sodium current, evoked and spontaneous action potentials determined by patch-clamp recording. (De) Quantification of iPSC-derived control and FRDA neurons participating in spontaneous calcium oscillations. (E) Loading of iPSC-derived neurons with the mitochondrial fluorescent dye TMRM. (Ea) Upper panels show representative fluorescent images of FRDA and control neuronal cultures loaded with TMRM. Lower panels show flow cytometry profile with TMRM fluorescence. (Eb) Quantification of mean fluorescence intensity in TMRM-positive cells in R2; $^{**}P<0.01$, $^{***}P<0.001$. (F) Electron microscopy analysis of FRDA iPSCs neurons at 43 days shows no ultrastructural abnormality. Fb is a higher magnification image of the boxed area shown in Fa; n, nucleus; m, mitochondria.

dependent sodium currents, four produced only a single action potential during step current injection, and none spontaneously generated action potentials (Fig. 3D). These findings suggest that, contrary to neurons from control iPSCs, neurons from FRDA iPSCs have not yet developed full electrophysiological functionality at 34-39 days of differentiation. However, when allowed additional time for maturation, FRDA iPSC-derived neurons eventually developed similar electrophysiological properties as control neurons. Accordingly, at 54-63 days of differentiation, 5/8 patched FRDA iPSC-derived neurons showed evoked action potentials and 3/8 had also spontaneous repetitive action potentials, similar to findings in control neurons (3/5 showing both evoked and spontaneous repetitive action potentials)

We next estimated mitochondrial integrity and functionality of neurons from FRDA and control iPSCs by assessing their ability to incorporate the mitochondrial membrane-permeable fluorescent dye tetramethylrhodamine methyl ester (TMRM), which is readily sequestered by active mitochondria. Flow cytometry analysis of cells

treated with TMRM revealed that FRDA neural cultures at 44-49 days of differentiation had a 40% lower fluorescence than control cultures (Fig. 3E), indicating reduced mitochondrial membrane potential (ΔΨm), which could result from defects in mitochondrial respiratory chain function. Interestingly, ultrastructural analysis of FRDA-derived neurons at the same stage of differentiation showed no defect, in particular mitochondria were well preserved with intact cristae (Fig. 3F).

Differentiation of iPSCs into cardiomyocytes

As the majority of FRDA patient present cardiac defects, we asked whether cardiomyocytes derived from FRDA iPSCs exhibit typical pathophysiological features of the disease. To generate cardiomyocytes, we adapted a protocol to induce differentiation relying on embryoid body (EB) formation combined with a treatment with ascorbic acid, a factor known to promote cardiac differentiation (Takahashi et al., 2003; Wang et al., 2010) (Fig. 4A). The yield of this differentiation protocol varied according to the iPSC line.

Spontaneously beating areas of variable morphology, size and pulse rate emerged around day 20 of differentiation (Fig. 4A; supplementary material Movies 2, 3). Cardiomyocytes at different degrees of maturation coexisted in the same area. qRT-PCR analyses confirmed the expression of cardiac lineage markers, as the transcription factor *GATA4*; *ACTN2* encoding the myofibrillar

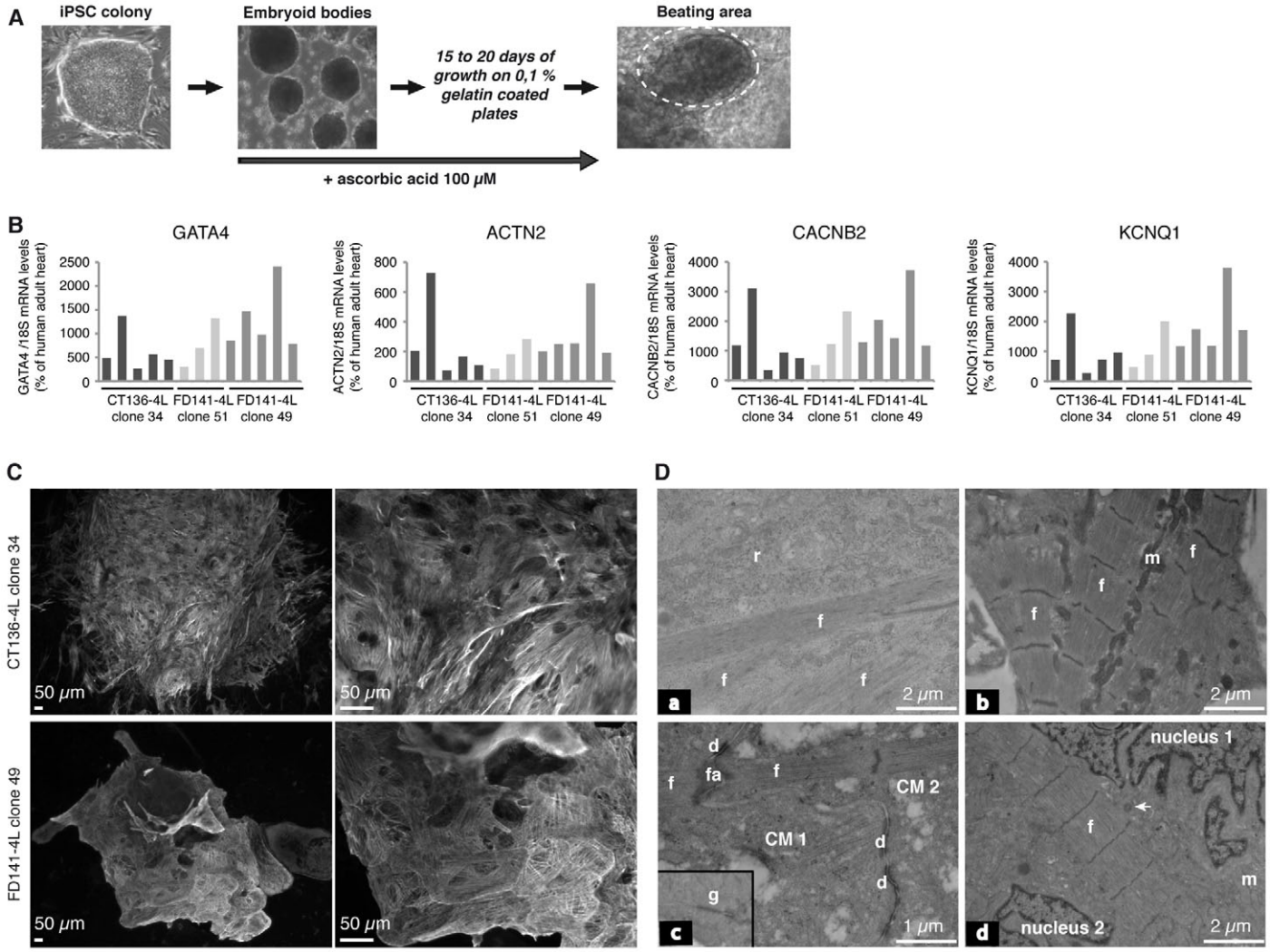

Fig. 4. Differentiation of iPSCs into cardiomyocytes and their characterisation. (A) Schematic view of the cardiomyocyte differentiation protocol with representative images showing an iPSC colony, EBs and a beating area (bright fields). (B) qRT-PCR analysis of cardiac marker expression relative to the *18S* housekeeping gene in different pools of beating areas from control (CT136-4L clone 34) and patient (FD141-4L clones 49 and 51) iPSCs, normalised to human adult heart. (C) Representative iPSC-derived beating areas from control (CT136-4L clone 34) and FRDA (FD141-4L clone 49) lines immunostained with cardiac troponin T to reveal cardiomyocyte organisation. (D) Representative electron microscopy images of iPSC-derived cardiomyocytes showing different degrees of structural maturity and intercellular junctions. (Da) Immature cardiomyocyte with organised contractile fibres or myofibrils without clear defined Z-line and with accumulation of ribosomes. (Db) Mature cardiomyocyte with dense myofibrillar sarcomeres bounded by straight dense Z-lines. Note that mitochondria are elongated and aligned in between myofibrils. (Dc) The presence of intercalated disks formed by desmosomes and fascia adherens, and occasionally gap junction (inset) connect different cardiomyocytes (CM1 and CM2). (Dd) Rare binucleated cardiomyocytes were observed (arrow points to centriole). d, desmosome; f, myofibril; fa, fascia adherens; g, gap junction; m, mitochondria; r, ribosome.

protein actinin α2; *CACNB2* encoding calcium voltage-dependent channel, beta 2 subunit; and *KCNQ1* encoding the potassium voltage-gated channel, KQT-like subfamily, member 1 (Fig. 4B; supplementary material Fig. S5). These genes were highly expressed in beating areas compared with adult cardiac mRNAs, reflecting the different degree of maturity. Cardiac troponin T immunostaining showed that the beating areas had comparable structure to heart tissue, with tightly imbricated but not aligned cardiomyocytes (Fig. 4C). Ultrastructural analysis revealed that early cardiomyocytes (<20 days) contained fibres already organised in beams, but only with Z-line drafts (Fig. 4Da). These cells also presented an accumulation of ribosomes and rough endoplasmic reticulum, indicating an intense protein synthesis activity, probably dedicated to building a mature contractile apparatus. With maturation, dense myofibrillar beams formed, with well-organised sarcomeres bounded by straight Z lines (Fig. 4Db). The presence of intercalated disks composed of adherent junctions, gap junctions and desmosomes (Fig. 4Dc) was indicative of an efficient contraction transmission within the beating areas. The majority of cardiomyocytes were mononucleated and a few were binucleated cardiomyocytes as normally observed in human heart (Fig. 4Dd).

FRDA cardiomyocytes recapitulate ultrastructural mitochondrial defects associated with FRDA

Cardiomyocytes derived from FRDA iPSCs retained the pathological GAA repeat expansions, but size heterogeneity was observed (Fig. 5A), possibly because samples from 12-22 beating areas were pooled to obtain sufficient material for genetic analyses. FRDA iPSC-derived cardiomyocytes maintained low levels (36-40%) of frataxin mRNA (Fig. 5A), but higher than in the original iPSCs (Fig. 1C; Fig. 5A), probably reflecting the contribution of beating areas with shorter GAA expansions.

We collected time-lapse images of 273 beating areas from several independent differentiation experiments to detect possible arrhythmias, as can occur in FRDA patients (Tsou et al., 2011). Surprisingly, we observed clonal differences, but no FRDA-related

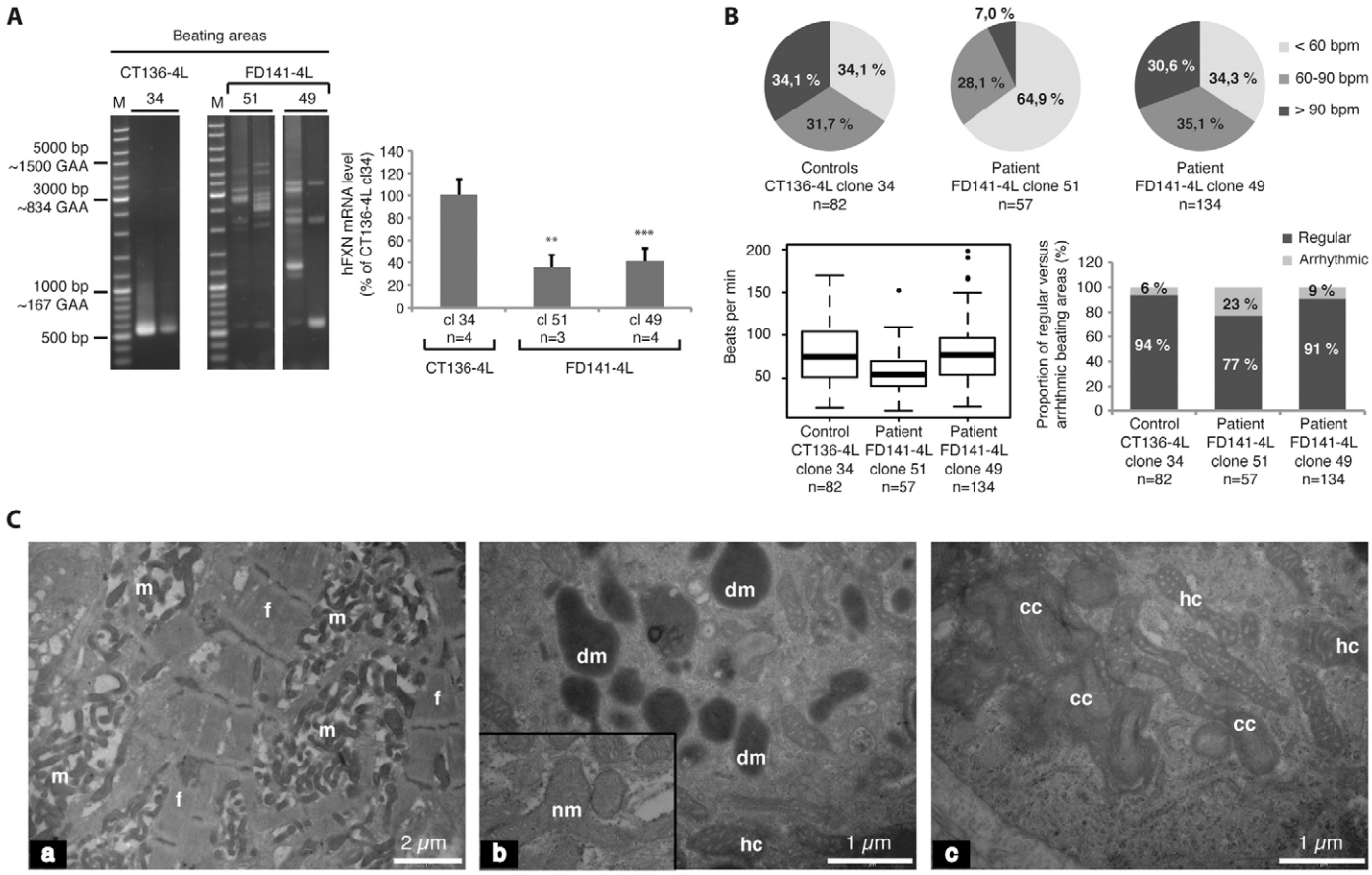

Fig. 5. FRDA cardiomyocytes present a mitochondrial phenotype. (A) PCR analysis of *FXN* GAA repeat length in representative pools of beating areas derived from control and FRDA iPSCs (left panel). qRT-PCR analysis of the expression levels of frataxin relative to *GADPH* in the pools of beating areas from control (CT136-4L clone 34) and FRDA (FD141-4L clones 49 and 51) iPSCs (right panel). The value of one pool of beating areas from the control was arbitrarily set to 100. The data are presented as mean ± s.d. ***P*<0.01, ****P*<0.001. (B) Analysis of the beating area contraction profiles by time-lapse imaging. Beating rate (beats per minutes; bpm) distribution (sectors and boxplot) and frequency of arrhythmic events (bars) are shown. The contraction rate distribution is categorised as slow (<60 bpm), intermediate (60-90 bpm) and fast (>90 bpm). (C) Ultrastructural changes in cardiomyocytes derived from FRDA iPSCs. No ultrastructural abnormality was observed in the organisation of the contractile fibre with clear defined sarcomeres. (Ca) Abnormal mitochondrial proliferation and/or accumulation. (Cb,c) Degenerating dark mitochondria with poorly defined cristae, mitochondria with hypertrophic cristae and onion-like mitochondria with coiled cristae. Inset: normal mitochondrion. cc, coiled cristae; dm, cristae; f, contractile fibre; hc, hypertrophic cristae; m, mitochondria; nm, normal mitochondrion.

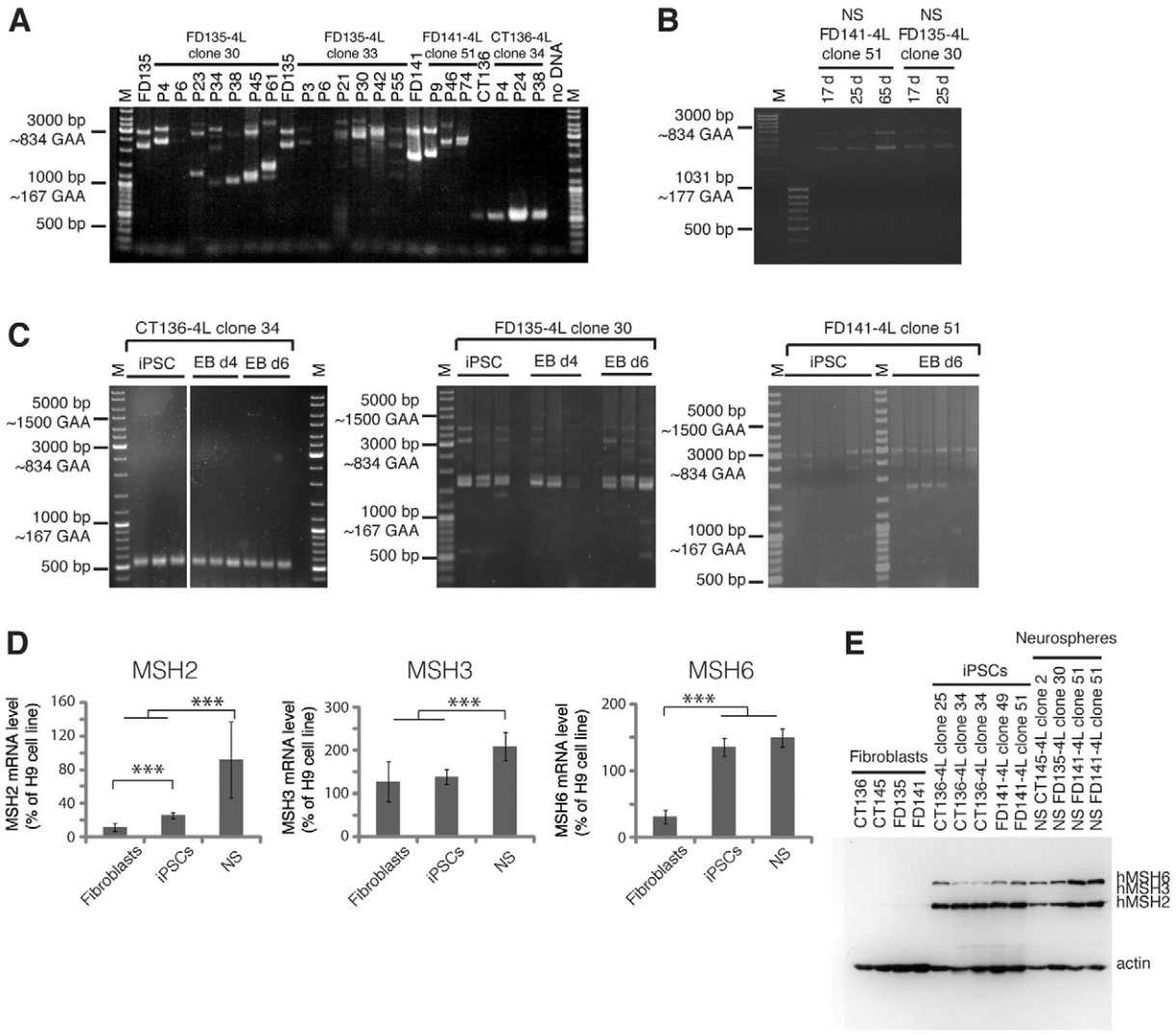

Fig. 6. iPSC show GAA instability over passages and increased expression level of mismatch repair enzymes. (A) PCR analysis of *FXN* GAA repeat length in fibroblast cell lines (FD135 and CT136) and iPSC clones from control and FRDA iPSCs at different passages (P#). M, molecular weight marker. (B) PCR analysis of *FXN* GAA repeat length in neurospheres. (C) PCR analysis of *FXN* GAA repeat length in EBs. (D) qRT-PCR analysis of *MSH2*, *MSH3* and *MSH6* expression in fibroblasts (n=8), iPSCs (n=6) and neurospheres (NS; at least 2 weeks of culture, n=7 from four different iPSC clones). No significant difference was seen between control and FRDA iPSC-derived cells. The data are represented as mean ± s.d. ***P<0.005. (E) Western blot analysis of total protein extracts from fibroblasts, iPSCs and neurospheres. Strong bands corresponding to MSH2 and MSH6 are detected in iPSCs and neurospheres; a weak band corresponding to MSH3 is detected in iPSCs and neurospheres (see supplementary material Fig. S8 for longer exposure). Actin was used as a loading control.

difference. In particular, even though they were derived from the same FRDA patient (FD141), beating areas from clone 49 had similar rhythmicity as controls, with few arrhythmia events (Fig. 5B), whereas those from clone 51 were slower and more arrhythmic (Fig. 5B). Overall, more than 93% of the recorded arrhythmia events occurred in slow (<60 bpm) beating areas.

Despite the lack of common contractile properties, ultrastructural analyses showed two main types of mitochondrial abnormalities in all seven beating areas from two FRDA iPSC clones: first, a proliferation and/or accumulation of structurally normal mitochondria (Fig. 5Ca; supplementary material Fig. S6); and, second, degenerated mitochondria with a dark matrix and poorly defined, in some cases collapsed cristae (Fig. 5Cb; supplementary material Fig. S6). Such dark mitochondria were found in control cardiomyocytes at a much lower frequency. Additional abnormalities were mitochondria with enrolled or hypertrophic cristae (Fig. 5Cc; supplementary material Fig. S6). These findings parallel the mitochondria damages seen in cardiac tissues from FRDA patients and from FRDA mouse models (Michael et al., 2006; Seznec et al., 2005) and are characteristic for respiration-compromised mitochondria. Mitochondrial pathology first appeared in mature cardiomyocytes within young FRDA beating areas (>1 month), and eventually affected all cardiomyocytes in older beating areas, even the remaining immature ones (supplementary material Fig. S7). No abnormalities in any other organelle were observed.

GAA repeat instability in FRDA iPSCs

We observed GAA repeat instability upon reprogramming (Fig. 1A), consistent with previously reports of GAA instability in FRDA patient-derived iPSCs (Ku et al., 2010; Liu et al., 2011). Monitoring the expanded GAA repeats in FRDA iPSCs over several passages, we detected both expansions and contractions, whereas normal repeats in control iPSCs remained stable (Fig. 6A). By contrast, during neural differentiation of FRDA iPSCs, only minor differences in GAA repeat length were observed between the starting iPSCs, neurospheres and their neuronal progeny (Fig. 3B), as well as after passaging of the neurospheres up to 65 days in culture (Fig. 6B). These data suggest that repeat instability substantially decreases when iPSCs commit to the neural lineage. This apparent stabilisation of the GAA tract would be consistent with the differentiation-induced stabilisation of CTG instability in myotonic dystrophy type 1 (DM1)-derived hESCs (Seriola et al., 2011). The heterogeneity in GAA repeat sizes in FRDA cardiomyocytes (Fig. 5A) could be a consequence of heterogeneity in the starting iPSC clones or of repeat instability during differentiation. However, GAA repeats were stable during the 6 days of EB differentiation prior to plating (Fig. 6C).

Mismatch repair (MMR) enzymes have previously been reported to be implicated in somatic trinucleotide repeat instability (reviewed by López Castel et al., 2010). In particular, increased levels of the MMR factors MSH2 and MSH3 have been proposed to cause enhanced GAA repeat instability (Ezzatizadeh et al., 2012; Ku et al., 2010). mRNA levels of MMR enzymes MSH2 and MSH6, but not MSH3, markedly increased in iPSCs and in neurospheres compared with the donor fibroblasts (Fig. 6D). No difference was observed between control and FRDA-derived cells, demonstrating that this mRNA upregulation is not related to the FRDA state. Because MMR transcript levels do not always reflect the corresponding protein levels (Chang et al., 2000), MSH2, MSH3 and MSH6 protein levels were assessed. By western blot analysis, the MSH2, MSH3 and MSH6 proteins were not detected in the donor fibroblasts, but abundant levels of MSH2 and MSH6 were detected in both iPSCs and neurospheres (Fig. 6E). MSH3 protein expression remained low in iPSCs and neurospheres, but was detectable compared with fibroblasts (supplementary material Fig. S8). Thus, MSH2, MSH3 and MSH6 proteins are expressed at higher levels in both the undifferentiated iPSCs and neuronal precursors compared with the parental fibroblast cells.

DISCUSSION

In the present study, we report the generation and characterisation of FRDA-derived iPSCs, and their differentiation into neurons and cardiomyocytes. Although the generation of peripheral sensory neurons and spontaneous beating cells using distinct protocols have previously been reported for FRDA-derived iPSC lines (Liu et al., 2011), this is the first report that provides a phenotypic characterisation of the neurons and cardiomyocytes derived from FRDA iPSCs. FRDA iPSCs retained expanded GAA repeats and expressed low levels of frataxin, but they showed no obvious phenotype with respect to control iPSCs. Furthermore, although inter-clonal variation was seen in differentiation efficiency, there was no overall difference in the efficiency or timing of neural and cardiac differentiation between FRDA and control iPSCs, suggesting that a reduced amount of frataxin does not affect the initial commitment to neuronal or cardiac fate. However, we cannot exclude the possibility that differences might emerge if iPSC differentiation is directed towards specific neuronal fates, such as primary sensory neurons, known to be highly vulnerable in FRDA.

Despite their apparently normal differentiation and morphology, young (34-39 days of differentiation) FRDA iPSC-derived neurons showed poor excitability compared with control iPSC-derived neurons (Fig. 3). Older (54-63 days) FRDA iPSC-derived neurons showed essentially normal electrophysiology, suggesting that the differences observed at 34-39 days reflect delayed functional maturation rather than a general functional failure. It is tempting to correlate the delayed maturation with the reduced uptake of TMRM by FRDA iPSC-derived neurons, indicative of reduced mitochondrial membrane potential, which could result from a defect in respiratory chain function rather than proton leak. Such a defect in respiratory chain function could be a direct consequence of Fe-S enzyme deficiency or oxidative stress. However, we cannot exclude the possibility that the differences might be due to loss of sick, non-functional neurons. Importantly, these findings provide measurable parameters to evaluate the effect of potential therapeutics on neurons carrying the FRDA mutations.

Cardiomyocyte physiology did not significantly differ between control and FRDA iPSC-derived cells. Time-lapse analysis of spontaneously contracting beating areas revealed inter-clonal variation rather than a disease-specific phenotype. The beat rates measured in this study were similar to spontaneous rates previously reported (Yazawa et al., 2011). Interestingly, the majority of arrhythmia events occurred in slow beating clusters. As there was heterogeneity in GAA repeat size among the beating clusters, it would be interesting to determine whether the rhythmic abnormalities observed are linked to higher GAA triplet expansions. By contrast, the ultrastructural abnormalities of cardiomyocytes derived from all FRDA iPSCs faithfully recapitulated some features observed in FRDA patients and animal models of the disease (Michael et al., 2006; Seznec et al., 2005). In particular, FRDA iPSC-derived cardiomyocytes present progressive extensive mitochondrial proliferation and accumulate mitochondria with swollen or onion-like cristae and dark mitochondria, which are characteristic of respiration-compromised mitochondria, suggestive of a functional defect in cellular respiration. Conversely, sarcomere disorganisation and mitochondrial iron accumulation, observed both in FRDA patient autopsies and in late stages of the disease in conditional knockout mice (Michael et al., 2006; Seznec et al., 2005), were not apparent in FRDA iPSC-derived cardiomyocytes, suggesting that they recapitulate the very early molecular and cellular changes of FRDA cardiomyopathy.

Neuronal and cardiac dysfunctions develop over several years in FRDA patients or several months in FRDA mouse models; however, both neurons and cardiomyocytes derived from the FRDA iPSCs develop a phenotype suggestive of mitochondrial respiratory chain defect over a relatively short period of time in culture. We cannot exclude the possibility that culture-related stress conditions accelerate the development of FRDA related phenotype *in vitro*. It is well known that frataxin-deficient cells are vulnerable to stress conditions (Chantrel-Groussard et al., 2001; Jiralerspong et al., 2001; Wong et al., 1999). In any case, our results strongly support impairment of oxidative phosphorylation, which is likely

to be present as a result of impaired Fe-S cluster biogenesis and possibly oxidative stress, as the main player in FRDA pathogenesis, at least in its early stages. Importantly, our findings provide measurable parameters for evaluating the effect of potential therapeutics on neurons and cardiomyocytes carrying the FRDA mutations.

Similarly to previous reports (Ku et al., 2010; Liu et al., 2011), the expanded GAA repeat showed instability during the reprogramming process. In addition, upon propagation in culture, high instability was observed in all FRDA iPSC clones, yielding both expansions and contractions of the expanded GAA repeats, in contrast with only expansions observed upon passage in culture in previous reports (Du et al., 2012; Ku et al., 2010). This discrepancy correlates with the difference in the GAA repeat size in the reprogrammed fibroblasts. Indeed, in the present report, the sizes of the GAA repeats were 800/600 and 900/400, respectively, whereas the sizes of the repeats in iPSCs showing only repeat expansion with no contraction were 330/380 and 541/420, respectively (Du et al., 2012; Ku et al., 2010). Furthermore, we cannot exclude the possibility that different approaches used to derive iPSCs, such as retroviral transduction and the inclusion of c-Myc in the set of reprogramming factors, and the different culture conditions could play a role. However, although instability during culture passages was not addressed, it is notable that Liu et al., using a similar protocol including the c-Myc transgene in the set of reprogramming factors, observed both expansions and contractions upon reprogramming, with repeat sizes at 527/1058 and 751/1027, respectively (Liu et al., 2011). The repeat instability we observed therefore appears to be more similar to events arising in the somatic tissues of FRDA patients and distinct from the suggested instability in FRDA iPSCs resembling intergenerational expansion (Du et al., 2012; Ku et al., 2010).

Increased expression of the MMR factors is known to be involved in repeat instability (López Castel et al., 2010) and, more specifically, MSH2 and MSH3 have been proposed to promote GAA repeat instability (Du et al., 2012; Ezzatizadeh et al., 2012; Halabi et al., 2012; Ku et al., 2010). Accordingly, we found upregulation of MSH2 and MSH6, and possibly MSH3, in all iPSCs irrespective of their genotype, suggesting an overall activation of mismatch repair during reprogramming. Interestingly, GAA repeats became much more stable in EBs, neurospheres, neurons and possibly cardiomyocytes, even though neurospheres maintained comparable mRNA and protein levels of MSH2 and MSH6 as iPSCs. This suggests that, in addition to MMR, other factors are likely to be involved in GAA repeat instability. The high level of MSH2 and MSH6 in neurospheres contrasts with a very recent report demonstrating that MSH2, MSH3 and MSH6 are expressed at lower levels in neural stem cells than in iPSCs (Du et al., 2012). Although no obvious explanation can explain this discrepancy, we observed high levels of MSH2 and MSH6 in neurospheres derived from three distinct iPSC clones, whereas Du et al. reports results for a unique clone (Du et al., 2012). Limited sample availability precluded MMR expression analysis in neurons and cardiomyocytes; however, previous reports indicate that MMR genes are downregulated and proteins are degraded upon differentiation (Seriola et al., 2011).

In conclusion, we show that iPSCs from FRDA patients maintain expanded GAA repeats and low expression of frataxin, and that iPSC-derived cardiomyocytes and neurons show pathological phenotypes that can be attributed to mitochondrial dysfunction. iPSCs represent a precious resource for studying the pathogenesis of FRDA and testing the effect of potential therapeutics. The major current limitation of this approach is the lack of robust protocols to obtain the most severely affected neuronal types in FRDA, such as large proprioceptive primary sensory neurons and deep cerebellar nuclei projection neurons, but it is reasonable to assume that these will be developed in the future.

MATERIALS AND METHODS

Human iPSC generation and characterisation

Human iPSCs were obtained as previously described (Lapillonne et al., 2010). For more clarity, to distinguish control and FRDA iPSC-derived cells; the original FD136 fibroblasts have been renamed as CT136 and the original iPSC clone FD136-25 as CT136-4L clone 25. Human iPSC characterisation was performed as previously described (Lapillonne et al., 2010). Supplementary material Table S1 gives a summary of the different analyses performed on each iPSC clone.

Molecular analysis

To determine GAA size, genomic DNA was extracted as previously described (Pandolfo, 2006). For the beating areas, DNA and RNA were extracted from the same sample using the RNA XS extraction kit (Macherey Nagels) and the Nucleospin RNA/DNA buffer set extension, according to the manufacturer's instructions. Beating area pellets were made of 12-22 beating areas, according to their age and size. PCR was performed on 10 ng of genomic DNA using the forward 5′-GGCTTGAACTTCCCACACGTGTT-3′ and reverse 5′-AGGACCATCATGGCCACACTT-3′ primers with the Expand Long Template PCR System Kit (Roche) in 50 µl reaction following the manufacturer's instructions. Then, 10 µl of the PCR sample was loaded on 1% agarose gel.

RNA was extracted with either TRI Reagent (MRC) or Nucleospin RNA XS (Macherey Nagel) following the manufacturer's recommendations and treated with Dnase I (Roche Biosciences). cDNA was generated using Superscript II kit (Invitrogen) and oligo-dT. Quantitative RT-PCR (qRT-PCR) was achieved using Light Cycler 480 (Roche Biosciences) with the primers listed in supplementary material Table S2 and, unless indicated, using GAPDH as internal standard. Total RNA from human adult heart tissue (Clontech) was used to evaluate mRNA expression levels in iPSC-derived cardiomyocytes. Beating area pellets were made of 12-22 beating areas, according to their age and size.

Transgene-specific primers were drawn to address reprogramming factor expression (supplementary material Table S2). Each gene-specific forward primer was used in couple with the same reverse primer picked up in IRES sequence immediately in 3′ of ORF. The double ΔCt method was used to quantify transgene expression, with primary human dermal fibroblasts infected with same viruses at MOI 10, as a calibrator. Negative controls were H9 hESC and original fibroblast cells. To avoid monitoring the potential expression of the transgenes, expression of endogenous Oct4, Nanog, Sox2 and Lin 28 was performed using primers designed in the 3′ untranslated region. HuES1 and H9 RNA were kindly provided by Olivier Pourquié (IGBMC, Illkirch, France).

In vitro differentiation analysis

Differentiation markers were analysed using Taqman Low Density Arrays (Life Technologies) as previously described (Lapillonne et al., 2010).

DNA methylation profile

Genomic DNA purified from H9 human embryonic stem cells, human iPSC and original dermal fibroblasts were bisulphite-treated according to the kit manufacturer (Qiagen). Strand-specific PCR was then performed on POU5F1 promoter according to published protocols and primers (Freberg et al., 2007). After PCR product cloning, between 10 and 15 clones were sequenced to establish DNA methylation profiles.

Teratoma analysis

Human iPSCs clumps were recovered from dishes using collagenase IV and dispase treatment. After washing, every human iPSC line was subcutaneously injected in two SCID mice (750,000 iPSCs per mouse) and teratoma formation followed over 3 months. When tumours reached 1 cm wide, mice were sacrificed, the tumours fixed in 4% PFA and processed for histological analysis.

Neural induction and differentiation

For neural induction, iPSC colonies were treated with Noggin for 14 days as previously described (Dottori and Pera, 2008), then mechanically transferred and cultured in NBN media (neurobasal media A+B27+N2) in the presence of FGF-2 and EGF (both 20 ng/ml; Peprotech, UK), which allowed the formation of neurospheres. Neural precursors were maintained and propagated as neurospheres by the cutting method and by replacing 50% of the medium every 2 days. For neuronal differentiation, neurospheres were plated on laminin-coated glass coverslips in NBN media without proliferating factors. To promote neuronal differentiation, brain-derived neurotrophic factor (BDNF) and neurotrophin 3 (NT3) (both 100 ng/ml; Peprotech, UK) were added in differentiating media. Within 3 days, neurospheres displayed signs of differentiation as they started extending processes in all directions.

Calcium imaging

For calcium dye loading, each coverslip containing differentiating neurospheres was incubated at 37°C for 45 minutes in the presence of 3 μM Oregon Green BAPTA 1 am (Life Technologies, Gent, Belgium). Imaging was carried out at room temperature using an upright Axioskop 2 microscope (Zeiss, Oberkochen, Germany) equipped with a CCD camera (iXon +, Andor). Images were acquired using a 63x, 0.95 NA water-immersion objective (Zeiss, Oberkochen, Germany). To excite the fluorescence of the calcium dye, a light source composed of a LED array (OptoLED, Cairn) emitting at 488 nm was coupled to the microscope equipped with a dichroic mirror and a high-pass emission filter centred at 505 and 507 nm, respectively. Using the AndorIQ software, images were acquired every 2 seconds, with an exposure time of 50 milliseconds and with a resolution of 512×512 pixels (14 bits). The pseudo ratio ($\Delta F/F$) curves corresponding to the different cells were computed offline. The fluorescence change over time is defined as $\Delta F/F=(F-F_{basal})/F_{basal}$, where F is the fluorescence at any time point, and F_{basal} is the baseline fluorescence averaged over three consecutive images at the beginning of the recording. The results presented here were obtained from three different coverslips (generated from two or three different experiments) cultured for 34-39 days.

Electrophysiology

Whole-cell patch clamp recordings were performed on individual neurons identified by using infrared differential interference contrast microscopy (Axioskop 2FS, 63× 0.95w, Zeiss). Recording pipettes were pulled from borosilicate glass capillaries (Hilgenberg, Malsfeld, Germany) on a PiP5 pipette puller (HEKA, Lambrecht-Pfalz, Germany) and presented resistances of 5-8 MOhm when filled with the patch pipette solutions containing the following: 119 mM $KMeSO_4$, 1 mM $MgCl_2$, 0.1 mM $CaCl_2$, 10 mM HEPES, 1 mM EGTA, 12 mM phosphocreatine, 2 mM Na_2ATP, 0.7 mM Na_2GTP, pH 7.2-7.3 adjusted with KOH, 280-300 mOsm/l. The extracellular solution contained: 126 mM NaCl, 1.6 mM KCl, 2 mM $CaCl_2$, 1 mM $MgCl_2$, 18 mM $NaHCO_3$, 1.2 mM KH_2PO_4 and 11 mM glucose, equilibrated with 95% O_2 and 5% CO_2 (pH 7.4). For the recordings, the glass coverslips were transferred into a recording chamber where they were continuously perfused (2-3 ml/min) with the extracellular solution at room temperature. All recordings were made with an Dual EPC10 amplifier and acquired using the software PatchMaster (HEKA). Signals were filtered at 4 kHz using the built-in filter of EPC10 and digitally sampled at 20 kHz. Data were analysed with Igor Pro software (WaveMetrics, Lake Oswego, OR). Passive cellular parameters were extracted in voltage clamp by analysing current relaxation induced by a 10-mV hyperpolarising step from a holding potential of –70 mV.

Measurement of mitochondrial membrane potential

Mitochondrial membrane potential changes ($\Delta\Psi m$) were detected using the slow, lipophilic, cationic fluorescent redistribution dye tetramethylrhodamine methyl ester (TMRM). Neurosphere-derived differentiated cells at 6 to 7 weeks old were dissociated by accutase and loaded with 25 nM TMRM (Life Technologies, Gent, Belgium) for 30 minutes at 37°C. In this experiment, TMRM was used in the 'redistribution mode' to assess $\Delta\psi_m$, and therefore a reduction in mitochondria-localised TMRM fluorescence represents mitochondrial depolarisation (Abramov et al., 2010). The mean fluorescence intensity was quantified using flow cytometry. Optimal emission from TMRM lies in the FL2 emission region (573 nm) and mean fluorescence of all test samples was measured with the FACScalibur flow cytometer (BD Biosciences) using the same voltage settings as determined for the negative control.

Cardiac differentiation

For cardiac differentiation, iPSC colonies were harvested after a 30 minutes of treatment with a mix of 1mg/ml collagenase IV (Invitrogen, France) and 2 mg/ml dispase (Invitrogen, France) at 37°C. EBs were formed by culturing small clumps of iPSC colonies in ultra-low attachment plates (Corning, France) for 6 days in DMEM-Ham F12 (1:1) supplemented with 20% KO-serum replacement (KSR), 1% non-essential amino acids, 1% penicillin-streptomycin, 1% glutamax and 0.1 mM 2-mercaptoethanol (all from Gibco, France). EBs were then plated onto 0.1% gelatin-coated plates in the same medium with a progressive replacement of KSR by foetal calf serum (PAA). Cardiac differentiation was

enhanced by adding 100 μM of ascorbic acid (Sigma, France) starting from day 1. First beating areas appeared around day 20 of differentiation.

Analysis of contraction rhythm in cardiomyocytes

Images were collected by time lapse every 68 or 26 milliseconds using Metamorph software and converted to multiframe TIFF images. Contraction profiles were built with ImageJ software by assessing the motion of light spots both in space and time. We calculated the ratio of the standard deviation to the mean of the intervals between 20 contractions, as described (Yazawa et al., 2011). The threshold for classifying a beating area as arrhythmic was a ratio at least two times higher than the average ratio of control cells.

Immunofluorescence

Full beating areas were rinsed with PBS and fixed in PBS containing 4% paraformaldehyde for 15 minutes at room temperature. Cells were blocked and permeabilised at the same time with PBS (10% NGS, 0.1% BSA, 0.1% Triton X-100) for 2 hours at room temperature. They were then incubated overnight at 4°C with the anti-cTnT primary antibody (1:200; MS-295-P0 from Fisher Scientific) diluted in PBS, 10%NGS, 0.1%BSA, 0.1%Triton X-100. The Alexa Fluor 488 goat anti-mouse secondary antibody (1:1000; Invitrogen) was incubated at room temperature for 1 hour. Immunofluorescence on neurospheres and neurons was performed as previously described (Chintawar et al., 2009). Briefly, to test their ability to express neural stem cell markers, neurospheres were plated on glass coverslips coated with matrigel (BD Biosciences, Erembodegem, Belgium), left overnight and then fixed with 4% paraformaldehyde. Triton X-100-permeabilised cultures were incubated with Nestin and SOX2 (Merck Millipore, Overijse, Belgium) antibodies overnight. For differentiating cultures, β-tubulin-III (Merck Millipore, Overijse, Belgium) and MAP2 (Sigma-Aldrich, Bornem, Belgium) were used as neuronal markers. Synapsin1 and VGlut1/2 (Synaptic Systems, Goettingen, Germany) were used to reveal synapses and vesicular glutamate transporters, respectively. The appropriate secondary antibodies coupled to Cy3 and FITC fluorochromes revealed the signal. In all the cultures, DAPI (4′,6-diamidino-2-phenylindole) was used to counterstain cell nuclei. Slides were mounted using Fluorsave (Calbiochem, Germany). Cultures were visualised either by laser scanning confocal microscope (LSM 510 META) or by AxioImager Z1 microscope (Zeiss, Jena, Germany). Exported images from LSM and Axiovison software were processed with the ImageJ (NIH) program and exported as TIFF files.

Immunoblot

Whole-cell protein extract of human iPSCs were made from frozen pellets by a lysis performed in TGEK-50 buffer (50 mM Tris HCl pH 7.4, 10% glycerol, 1 mM EDTA, 50 mM KCl) with 0.5% Triton X-100 and protease inhibitor (Complete-EDTA-free, Roche). From each sample, 25 μg of protein was electrophoresed in 14% SDS-PAGE and transferred onto nitrocellulose membranes. Primary antibodies (anti-frataxin, 1:250; 18A5DB1, Mitosciences; anti-β-tubulin, 1:40,000; IGBMC-made; anti-SDH (su30kDa), 1:1000; Invitrogen; anti-NDUFS3, 1:2000; Invitrogen; anti-lipoid acid, 1:5000; Calbiochem; and anti-GAPDH, 1:20,000; IGBMC-made) were incubated overnight at 4°C. HRP-conjugated secondary antibody (goat anti-mouse or anti-rabbit, 1:5000; Jackson ImmunoResearch) was incubated for 1 hour at room temperature. Immunocomplexes were revealed by SuperSignal West Pico or Dura Chemiluminescent Substrate (37071, Pierce), according to the manufacturer's instructions.

For mismatch repair protein analysis, cells were resuspended in (0.125 M Tris-HCl pH 6.8, 4% SDS, 10% glycerol) containing Protease Inhibitor Cocktail (Roche) and sonicated for 45 seconds. Protein concentration was determined using the Pierce BCA protein assay kit. Proteins (40 μg) were denatured for 5 minutes at 95°C in 4× loading buffer and resolved by electrophoresis on an 8% polyacrylamide SDS-PAGE gel. Membranes were blocked for 1 hour at room temperature in PBS-T containing 5% (m/v) dried milk. Primary MMR antibodies were incubated simultaneously overnight at 4°C in antibodies anti-MSH2 (1:2800; NA27, Calbiochem), anti-MSH6 (1:2000; 610918, BD Laboratories), anti-MSH3 (1:2000; 611930, BD Laboratories) and anti-Actin Ab-5 (1:20,000; 612656, BD Laboratories). The membranes were incubated for 1 hour in secondary antibody (sheep anti-mouse-HRP, 1:5000; 515-035-062, Jackson ImmunoResearch) at room temperature and visualised using ECL plus western blotting detection system (RPN2132, Amersham).

Enzyme activities

iPSCs were harvested with collagenase IV and dispase (Invitrogen) in PBS and the dry pellet immediately frozen at –80°C. The activity of the respiratory chain enzyme complex succinate dehydrogenase (SDH, complex II) and the citric acid cycle enzymes isocitrate dehydrogenase (IDH) were determined as previously described (Calmels et al., 2009).

Electron microscopy

Cells were fixed in 2.5% paraformaldehyde and 2.5% glutaraldehyde in cacodylate buffer (0.1 M, pH 7.2), rinsed in cacodylate buffer and postfixed in 1% osmium tetroxide in 0.1 M cacodylate buffer for 1 hour at 4°C. Cells were contrasted with uranyl acetate for 2 hours at 4°C, dehydrated, and embedded in Epon. Ultrathin sections were cut at 70 nm and contrasted with uranyl acetate and lead citrate and examined with a Morgagni 268D electron microscope.

Statistics

Results are represented as mean ± s.d. Comparisons between groups for mean fluorescence intensity were made using one way analysis of variance (ANOVA) followed by Bonferroni post-hoc test using the Prism Software (GraphPad Software). Histograms were generated using Sigmaplot 10.0. All histograms and images generated using ImageJ software (NIH) were imported in Adobe Illustrator and the final figure was exported in TIFF format. *P*-values less than 0.05 were considered significant.

ACKNOWLEDGEMENTS

We thank Marcel Boeglin, Josiane Hergueux, Laetitia Fuhrman and Jean-Luc Weickert from the IGBMC for technical help. We thank Eric Jeandidier (CHU Mulhouse) for iPSCs caryotypes. We thank Karim Hnia, Alain Martelli and Karine Merienne for helpful discussion and reading through the manuscript.

COMPETING INTERESTS

The authors declare that they do not have any competing or financial interests.

AUTHOR CONTRIBUTIONS

A.H. designed and performed experiments for iPSC characterisation, differentiation and characterisation of cardiomyocytes from iPSCs. M.W.-D. designed and performed experiments for iPSC derivation and characterisation, neurospheres and neurons from iPSCs. S.C. designed and performed experiments for the differentiation and characterisation of neurospheres and neurons from iPSCs. P.T. designed strategy and performed experiments for iPSCs derivation. J.P.S. performed the mismatch repair western blot. N.V., D.G., L.L., C.A., L.R. and M.R. performed experiments. M.T. was responsible for the teratoma analysis. N.M. was responsible for electron microscopy studies. S.N.S. designed the electrophysiological studies. S.V. designed the iPSC derivation. C.E.P. designed the mismatch repair study. M.P. and H.P. conceived, designed and supervised the complete study. A.H., M.W.-D., S.C., M.P. and H.P. wrote the manuscript. All authors read and approved the content of the manuscript.

FUNDING

This work was supported by the US Friedreich's Ataxia Research Alliance (USA) (to H.P. and to M.P.), the Association Française pour l'Ataxie de Friedreich (to H.P.), the Association Française contre les Myopathies (to S.V.), the Ministère de l'économie, de l'industrie et de l'emploi (to S.V.), and the European Community under the European Research Council [grant number 206634/ISCATAXIA to H.P.] and the 7th Framework Program [grant number 242193/EFACTS to H.P. and to M.P.].

SUPPLEMENTARY MATERIAL

Supplementary material for this article is available at
http://dmm.biologists.org/lookup/suppl/doi:10.1242/dmm.010900/-/DC1

REFERENCES

Abramov, A. Y., Smulders-Srinivasan, T. K., Kirby, D. M., Acin-Perez, R., Enriquez, J. A., Lightowlers, R. N., Duchen, M. R. and Turnbull, D. M. (2010). Mechanism of neurodegeneration of neurons with mitochondrial DNA mutations. *Brain* **133**, 797-807.

Al-Mahdawi, S., Pinto, R. M., Varshney, D., Lawrence, L., Lowrie, M. B., Hughes, S., Webster, Z., Blake, J., Cooper, J. M., King, R. et al. (2006). GAA repeat expansion mutation mouse models of Friedreich ataxia exhibit oxidative stress leading to progressive neuronal and cardiac pathology. *Genomics* **88**, 580-590.

Calmels, N., Schmucker, S., Wattenhofer-Donzé, M., Martelli, A., Vaucamps, N., Reutenauer, L., Messaddeq, N., Bouton, C., Koenig, M. and Puccio, H. (2009). The first cellular models based on frataxin missense mutations that reproduce spontaneously the defects associated with Friedreich ataxia. *PLoS ONE* **4**, e6379.

Campuzano, V., Montermini, L., Moltò, M. D., Pianese, L., Cossée, M., Cavalcanti, F., Monros, E., Rodius, F., Duclos, F., Monticelli, A. et al. (1996). Friedreich's ataxia: autosomal recessive disease caused by an intronic GAA triplet repeat expansion. *Science* **271**, 1423-1427.

Campuzano, V., Montermini, L., Lutz, Y., Cova, L., Hindelang, C., Jiralerspong, S., Trottier, Y., Kish, S. J., Faucheux, B., Trouillas, P. et al. (1997). Frataxin is reduced in Friedreich ataxia patients and is associated with mitochondrial membranes. *Hum. Mol. Genet.* **6**, 1771-1780.

Chang, D. K., Ricciardiello, L., Goel, A., Chang, C. L. and Boland, C. R. (2000). Steady-state regulation of the human DNA mismatch repair system. *J. Biol. Chem.* **275**, 18424-18431.

Chantrel-Groussard, K., Geromel, V., Puccio, H., Koenig, M., Munnich, A., Rötig, A. and Rustin, P. (2001). Disabled early recruitment of antioxidant defenses in Friedreich's ataxia. *Hum. Mol. Genet.* **10**, 2061-2067.

Chintawar, S., Hourez, R., Ravella, A., Gall, D., Orduz, D., Rai, M., Bishop, D. P., Geuna, S., Schiffmann, S. N. and Pandolfo, M. (2009). Grafting neural precursor cells promotes functional recovery in an SCA1 mouse model. *J. Neurosci.* **29**, 13126-13135.

Clark, R. M., De Biase, I., Malykhina, A. P., Al-Mahdawi, S., Pook, M. and Bidichandani, S. I. (2007). The GAA triplet-repeat is unstable in the context of the human FXN locus and displays age-dependent expansions in cerebellum and DRG in a transgenic mouse model. *Hum. Genet.* **120**, 633-640.

Cnop, M., Igoillo-Esteve, M., Rai, M., Begu, A., Serroukh, Y., Depondt, C., Musuaya, A., Marhfour, I., Ladrière, L., Moles Lopez, X. et al. (2012). The central role and mechanisms of β-cell dysfunction and death in Friedreich's ataxia-associated diabetes. *Ann. Neurol.* [Epub ahead of print] doi: 10.1002/ana.23698.

De Biase, I., Rasmussen, A., Monticelli, A., Al-Mahdawi, S., Pook, M., Cocozza, S. and Bidichandani, S. I. (2007). Somatic instability of the expanded GAA triplet-repeat sequence in Friedreich ataxia progresses throughout life. *Genomics* **90**, 1-5.

Deutsch, E. C., Santani, A. B., Perlman, S. L., Farmer, J. M., Stolle, C. A., Marusich, M. F. and Lynch, D. R. (2010). A rapid, noninvasive immunoassay for frataxin: utility in assessment of Friedreich ataxia. *Mol. Genet. Metab.* **101**, 238-245.

Dottori, M. and Pera, M. F. (2008). Neural differentiation of human embryonic stem cells. *Methods Mol. Biol.* **438**, 19-30.

Du, J., Campau, E., Soragni, E., Ku, S., Puckett, J. W., Dervan, P. B. and Gottesfeld, J. M. (2012). Role of mismatch repair enzymes in GAA·TTC triplet-repeat expansion in Friedreich ataxia induced pluripotent stem cells. *J. Biol. Chem.* **287**, 29861-29872.

Ezzatizadeh, V., Pinto, R. M., Sandi, C., Sandi, M., Al-Mahdawi, S., Te Riele, H. and Pook, M. A. (2012). The mismatch repair system protects against intergenerational GAA repeat instability in a Friedreich ataxia mouse model. *Neurobiol. Dis.* **46**, 165-171.

Freberg, C. T., Dahl, J. A., Timoskainen, S. and Collas, P. (2007). Epigenetic reprogramming of OCT4 and NANOG regulatory regions by embryonal carcinoma cell extract. *Mol. Biol. Cell* **18**, 1543-1553.

Guillon, B., Bulteau, A. L., Wattenhofer-Donzé, M., Schmucker, S., Friguet, B., Puccio, H., Drapier, J. C. and Bouton, C. (2009). Frataxin deficiency causes upregulation of mitochondrial Lon and ClpP proteases and severe loss of mitochondrial Fe-S proteins. *FEBS J.* **276**, 1036-1047.

Halabi, A., Ditch, S., Wang, J. and Grabczyk, E. (2012). DNA mismatch repair complex MutSβ promotes GAA·TTC repeat expansion in human cells. *J. Biol. Chem.* **287**, 29958-29967.

Jiralerspong, S., Ge, B., Hudson, T. J. and Pandolfo, M. (2001). Manganese superoxide dismutase induction by iron is impaired in Friedreich ataxia cells. *FEBS Lett.* **509**, 101-105.

Ku, S., Soragni, E., Campau, E., Thomas, E. A., Altun, G., Laurent, L. C., Loring, J. F., Napierala, M. and Gottesfeld, J. M. (2010). Friedreich's ataxia induced pluripotent stem cells model intergenerational GAA TTC triplet repeat instability. *Cell Stem Cell* **7**, 631-637.

Lapillonne, H., Kobari, L., Mazurier, C., Tropel, P., Giarratana, M. C., Zanella-Cleon, I., Kiger, L., Wattenhofer-Donzé, M., Puccio, H., Hebert, N. et al. (2010). Red blood cell generation from human induced pluripotent stem cells: perspectives for transfusion medicine. *Haematologica* **95**, 1651-1659.

Lill, R. (2009). Function and biogenesis of iron-sulphur proteins. *Nature* **460**, 831-838.

Liu, J., Verma, P. J., Evans-Galea, M. V., Delatycki, M. B., Michalska, A., Leung, J., Crombie, D., Sarsero, J. P., Williamson, R., Dottori, M. et al. (2011). Generation of induced pluripotent stem cell lines from Friedreich ataxia patients. *Stem Cell Rev.* **7**, 703-713.

López Castel, A., Cleary, J. D. and Pearson, C. E. (2010). Repeat instability as the basis for human diseases and as a potential target for therapy. *Nat. Rev. Mol. Cell Biol.* **11**, 165-170.

Mariani, J., Simonini, M. V., Palejev, D., Tomasini, L., Coppola, G., Szekely, A. M., Horvath, T. L. and Vaccarino, F. M. (2012). Modeling human cortical development in vitro using induced pluripotent stem cells. *Proc. Natl. Acad. Sci. USA* **109**, 12770-12775.

Martelli, A., Wattenhofer-Donzé, M., Schmucker, S., Bouvet, S., Reutenauer, L. and Puccio, H. (2007). Frataxin is essential for extramitochondrial Fe-S cluster proteins in mammalian tissues. *Hum. Mol. Genet.* **16**, 2651-2658.

Martelli, A., Napierala, M. and Puccio, H. (2012). Understanding the genetic and molecular pathogenesis of Friedreich's ataxia through animal and cellular models. *Dis. Model. Mech.* **5**, 165-176.

Michael, S., Petrocine, S. V., Qian, J., Lamarche, J. B., Knutson, M. D., Garrick, M. D. and Koeppen, A. H. (2006). Iron and iron-responsive proteins in the cardiomyopathy of Friedreich's ataxia. *Cerebellum* **5**, 257-267.

Miranda, C. J., Santos, M. M., Ohshima, K., Smith, J., Li, L., Bunting, M., Cossée, M., Koenig, M., Sequeiros, J., Kaplan, J. et al. (2002). Frataxin knockin mouse. *FEBS Lett.* **512**, 291-297.

Monrós, E., Moltó, M. D., Martínez, F., Cañizares, J., Blanca, J., Vílchez, J. J., Prieto, F., de Frutos, R. and Palau, F. (1997). Phenotype correlation and intergenerational dynamics of the Friedreich ataxia GAA trinucleotide repeat. *Am. J. Hum. Genet.* **61**, 101-110.

Navarro-Sastre, A., Tort, F., Stehling, O., Uzarska, M. A., Arranz, J. A., Del Toro, M., Labayru, M. T., Landa, J., Font, A., Garcia-Villoria, J. et al. (2011). A fatal mitochondrial disease is associated with defective NFU1 function in the maturation of a subset of mitochondrial Fe-S proteins. *Am. J. Hum. Genet.* **89**, 656-667.

Onder, T. T. and Daley, G. Q. (2012). New lessons learned from disease modeling with induced pluripotent stem cells. *Curr. Opin. Genet. Dev.* **22**, 500-508.

Pandolfo, M. (2006). Friedreich ataxia: Detection of GAA repeat expansions and frataxin point mutations. *Methods Mol. Med.* **126**, 197-216.

Pandolfo, M. (2009). Friedreich ataxia: the clinical picture. *J. Neurol.* **256 Suppl. 1**, 3-8.

Puccio, H., Simon, D., Cossée, M., Criqui-Filipe, P., Tiziano, F., Melki, J., Hindelang, C., Matyas, R., Rustin, P. and Koenig, M. (2001). Mouse models for Friedreich ataxia exhibit cardiomyopathy, sensory nerve defect and Fe-S enzyme deficiency followed by intramitochondrial iron deposits. *Nat. Genet.* **27**, 181-186.

Rötig, A., de Lonlay, P., Chretien, D., Foury, F., Koenig, M., Sidi, D., Munnich, A. and Rustin, P. (1997). Aconitase and mitochondrial iron-sulphur protein deficiency in Friedreich ataxia. *Nat. Genet.* **17**, 215-217.

Saveliev, A., Everett, C., Sharpe, T., Webster, Z. and Festenstein, R. (2003). DNA triplet repeats mediate heterochromatin-protein-1-sensitive variegated gene silencing. *Nature* **422**, 909-913.

Schmucker, S. and Puccio, H. (2010). Understanding the molecular mechanisms of Friedreich's ataxia to develop therapeutic approaches. *Hum. Mol. Genet.* **19**, R103-R110.

Schmucker, S., Martelli, A., Colin, F., Page, A., Wattenhofer-Donzé, M., Reutenauer, L. and Puccio, H. (2011). Mammalian frataxin: an essential function for cellular viability through an interaction with a preformed ISCU/NFS1/ISD11 iron-sulfur assembly complex. *PLoS ONE* **6**, e16199.

Selak, M. A., Lyver, E., Micklow, E., Deutsch, E. C., Onder, O., Selamoglu, N., Yager, C., Knight, S., Carroll, M., Daldal, F. et al. (2011). Blood cells from Friedreich ataxia patients harbor frataxin deficiency without a loss of mitochondrial function. *Mitochondrion* **11**, 342-350.

Seriola, A., Spits, C., Simard, J. P., Hilven, P., Haentjens, P., Pearson, C. E. and Sermon, K. (2011). Huntington's and myotonic dystrophy hESCs: down-regulated trinucleotide repeat instability and mismatch repair machinery expression upon differentiation. *Hum. Mol. Genet.* **20**, 176-185.

Seznec, H., Simon, D., Bouton, C., Reutenauer, L., Hertzog, A., Golik, P., Procaccio, V., Patel, M., Drapier, J. C., Koenig, M. et al. (2005). Friedreich ataxia: the oxidative stress paradox. *Hum. Mol. Genet.* **14**, 463-474.

Simon, D., Seznec, H., Gansmuller, A., Carelle, N., Weber, P., Metzger, D., Rustin, P., Koenig, M. and Puccio, H. (2004). Friedreich ataxia mouse models with progressive cerebellar and sensory ataxia reveal autophagic neurodegeneration in dorsal root ganglia. *J. Neurosci.* **24**, 1987-1995.

Takahashi, T., Lord, B., Schulze, P. C., Fryer, R. M., Sarang, S. S., Gullans, S. R. and Lee, R. T. (2003). Ascorbic acid enhances differentiation of embryonic stem cells into cardiac myocytes. *Circulation* **107**, 1912-1916.

Tsai, C. L. and Barondeau, D. P. (2010). Human frataxin is an allosteric switch that activates the Fe-S cluster biosynthetic complex. *Biochemistry* **49**, 9132-9139.

Tsou, A. Y., Paulsen, E. K., Lagedrost, S. J., Perlman, S. L., Mathews, K. D., Wilmot, G. R., Ravina, B., Koeppen, A. H. and Lynch, D. R. (2011). Mortality in Friedreich ataxia. *J. Neurol. Sci.* **307**, 46-49.

Wang, Y., Chen, G., Song, T., Mao, G. and Bai, H. (2010). Enhancement of cardiomyocyte differentiation from human embryonic stem cells. *Science China. Life Sci.* **53**, 581-589.

Wong, A., Yang, J., Cavadini, P., Gellera, C., Lonnerdal, B., Taroni, F. and Cortopassi, G. (1999). The Friedreich's ataxia mutation confers cellular sensitivity to oxidant stress which is rescued by chelators of iron and calcium and inhibitors of apoptosis. *Hum. Mol. Genet.* **8**, 425-430.

Yazawa, M., Hsueh, B., Jia, X., Pasca, A. M., Bernstein, J. A., Hallmayer, J. and Dolmetsch, R. E. (2011). Using induced pluripotent stem cells to investigate cardiac phenotypes in Timothy syndrome. *Nature* **471**, 230-234.

Ye, H. and Rouault, T. A. (2010). Human iron-sulfur cluster assembly, cellular iron homeostasis, and disease. *Biochemistry* **49**, 4945-4956.